ARTICLE   OPEN

Check for updates

MoCoB metallic glass microwire catalysts for highly efficient and pH-universal degradation of wastewater

Meifang Tang[1], Limin Lai[1], Chen Su[1], Chunmei Li[1], Cheng Zhang[2✉] and Shengfeng Guo[1✉]

One important goal of the current Fenton-like catalysts is to develop highly efficient and pH-universal catalysts that can operate with little performance degradation over multiple recycles. Herein, we report a ternary MoCoB metallic glass (MG) microwire catalyst, which shows exceptional Fenton-like activity for degrading various dyes in a wide pH range (5–10). Moreover, the MoCoB MG catalyst with an ultrahigh glass-transition temperature of 1002 K exhibits excellent reusability and can be used for more than 46 times without a decay in efficiency. It is regarded that the excellent catalytic activity and sustainability of the MoCoB MG catalyst originates from the bimetallic effect involving Mo^n/Mo^{n+1} and Co^{n+1}/Co^n cycling, which accelerates the electronic transfer kinetics, enabling the generation of multiple reactive oxygen species ($\cdot OH$ and $\cdot O_2^-$). First-Principles Calculations revealed again that MG catalysts provide a large electron base for the whole catalytic process.

INTRODUCTION

Metallic glasses (MGs) exhibit excellent physical and chemical properties due to their atomic disordering arrangement and metastability[1]. MGs with simultaneously high catalytic activity and unique selectivity have emerged as a kind of competitive candidate catalyst for hydrogen evolution reaction (HER)[2,3], and oxygen evolution reaction (OER)[4], etc. Especially, their excellent catalytic performance in wastewater treatment has attracted increasing attention in recent years[5–7]. For example, the degradation efficiency of $Fe_{73}Si_7B_{17}Nb_3$ MG powders for Direct Blue 6 is 200 times higher than that of commercial iron powder[8]. The degradation efficiency of $Fe_{78}Si_9B_{13}$ and $Fe_{73.5}Si_{13.5}B_9Cu_1Nb_3$ MG ribbons is 5–10 times higher than that of their crystalline counterparts[9]. Beside Fe-based MG system, other MG systems (including Mg-based, Co-based) with high degradation efficiency have also been developed.

Although MGs have shown high catalytic activity in degrading dying wastewater, they still face several challenges and drawbacks. Firstly, most of the MG catalysts reported so far are mainly in the forms of ribbons, the small specific surface area of which usually limits their reactivity[10–12]. Secondly, a trade-off between the catalytic activity and long-term stability remains, that is, the active MG catalysts are not chemically stable while those stable MGs have low catalytic activity. This dilemma typically results in a limited reusability (normally <35 times[13]). For instance, the catalytic process of the FeSiB MG is always accompanied with surface aging and corrosion, resulting in progressively decreased catalytic efficiency and reaction rate constant (k_{obs}) decreases progressively with the number of cycles[14,15]. Furthermore, most MGs can only degrade dyes in a narrow pH ranges (2–3.5), and a small change in pH value will cause drastic decay in the degradation rate[16–18]. Although some MG catalyst has been reported to be operate in a wide pH range, the degradation efficiency is actually extremely slow, e.g., the complete degradation of a Direct Blue 2B requires more than 100 h[19]. Since the industry applications usually involve with neutral or alkaline condition, it is necessary to develop highly reusable, efficient, and pH-universal MG catalysts.

In this work, we demonstrate that a ternary MoCoB MG microwire can be a highly active and stable catalysts for Fenton-like reactions. We found the $Mo_{51}Co_{34}B_{15}$ MG can exhibit high degradation efficiency towards various dying wastewater within a wide pH range (5–10), and shows negligible degradation after operation for 45 times. We attribute the notable catalytic performance of this $Mo_{51}Co_{34}B_{15}$ MG to Crystal Violet (CV) dye, as well as the large specific surface area of microwires.

RESULTS AND DISCUSSION

Synthesis of MoCoB MG microwire and their characterization

Figure 1a shows a schematic diagram of designing and preparing MG microwire using melt-spinning techniques, raising the micro-sized tube to bring the metal liquid contacted with the edge of the sharp copper rod. The as-fabricated MG wires can be seen in Fig. 1b, and the surface of the prepared $Mo_{51}Co_{34}B_{15}$ MG microwire is very smooth, as shown in Fig. 1c. The XRD pattern in Fig. 1d exhibits a broad diffuse scattering peak of 43°, without obvious crystalline peaks, indicating the fully amorphous structure within the resolution limit of XRD. The DTA curve shown in Fig. 1e shows that the $Mo_{51}Co_{34}B_{15}$ MG wires have an obvious glass transition and multi-step crystallization reaction, which further confirms its amorphous nature[20,21]. It should be noted that the present $Mo_{51}Co_{34}B_{15}$ MG catalyst exhibits an ultra-high glass transition temperature T_g (1002 K) and crystallization temperature T_x (1070 K), which is far higher than those of FeSiB MG catalysts ($T_g = 693$ K)[22]. The excellent thermal stability could endow the MG with long-term stability and reusability under harsh (e.g., high-temperature) wastewater treatment conditions. The specific surface area (SSA) of the MG microwires catalyst is 5.9 m^2/g (Fig. 1f), which is 1–2 orders of magnitude higher than that of most reported MG ribbons[23]. The high SSA is beneficial for exposing more abundant active sites for catalytic reactions.

[1]School of Materials and Energy, Southwest University, 400715 Chongqing, China. [2]School of Materials Science and Engineering, State Key Lab for Materials Processing and Die & Mold Technology, Huazhong University of Science and Technology, 430074 Wuhan, China. ✉email: czhang@hust.edu.cn; sfguo@swu.edu.cn
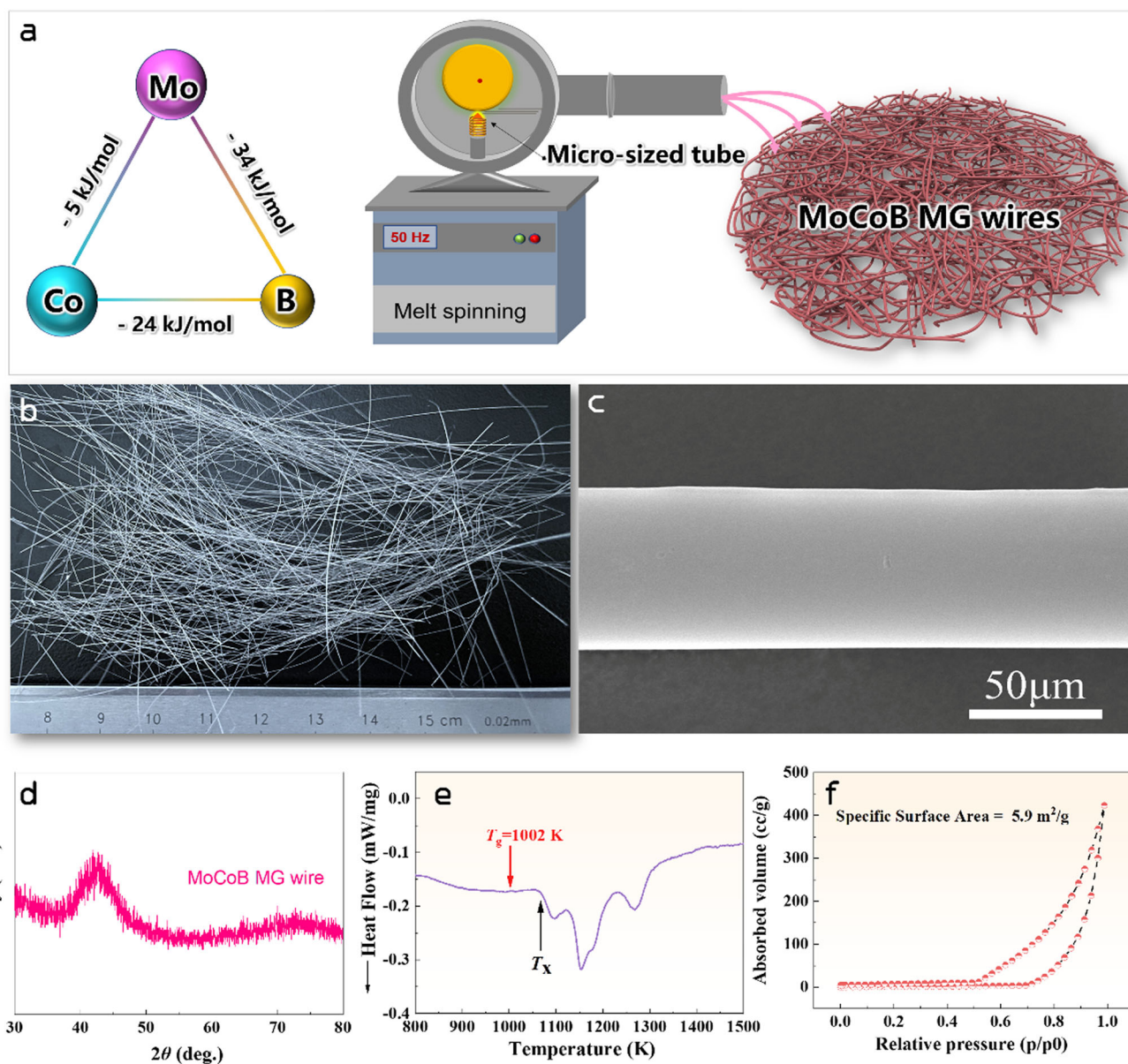
Fig. 1 **Catalysts structure. a** Schematic illustration of the preparing processes of MoCoB MG microwires. **b** Photographs of prepared microwire. **c** SEM image, **d** XRD pattern, **e** DTA curve, **f** Isothermal adsorption and desorption curves of the prepared MoCoB MG wires, respectively.

Catalytic performance

The catalytic performance of the $Mo_{51}Co_{34}B_{15}$ MG wire catalysts was assessed via degradation of CV solutions (a typical triarylmethane dye in industry). It is found that the current MoCoB MG wires show superior catalytic activity than the typical FeSiB MG ribbons (Fig. 2a), the MoCoB catalysts achieved 99% degradation of the CV solution within 20 min, whereas the latter was only 50%. The degradation reaction follows the pseudo-first-order kinetic model, k_{obs} can be obtained from Eq. (1)

$$\ln(C_0/C_t) = k_{obs}t \qquad (1)$$

where C_0 is the initial concentration of dye, C_t is the concentration at t, and t is the reaction time. The calculated k_{obs} value of $Mo_{51}Co_{34}B_{15}$ is about 7 times higher than that of $Fe_{78}Si_9B_{13}$, again indicating the excellent degradation performance of the current catalyst. To verify the versatility of the microwire catalysis, three typical dyes of Crystal Violet, Malachite Green and Direct Blue 6 were selected for degradation experiments. As shown in Fig. 2b, Crystal Violet and

Direct Blue 6 could be completely removed by the MoCoB wire catalyst within 15 min, and Malachite Green become completely colorless within 10 min. Interestingly, we find that, in our sample of MoCoB MG wire exhibits excellent adaptability to pH changes. It achieves complete degradation of most acidic and alkaline solutions, with a rapid and effective degradation at pH 5–10 (Fig. 2c). This greatly breaks the pH limitation of metallic glasses for dyes degradation and can effectively address the critical issue of degradation under alkaline conditions[24,25]. Interestingly, unlike other metallic glasses, the degradation rate of current MG microwire catalysts accelerates with increasing pH value of the solution. The breaking of the trade-off between pH and catalytic activity indicates that a catalytic mechanism for this MoCoB MG catalyst, which will be discussed later. To further highlight the excellent catalytic performance of this catalyst, the comparable results of applicable pH value versus k_{obs} for various MG catalysts in wastewater treatment are summarized[9,15–17,26–31] (Fig. 2d), more details can be found at Supplementary Table 1.
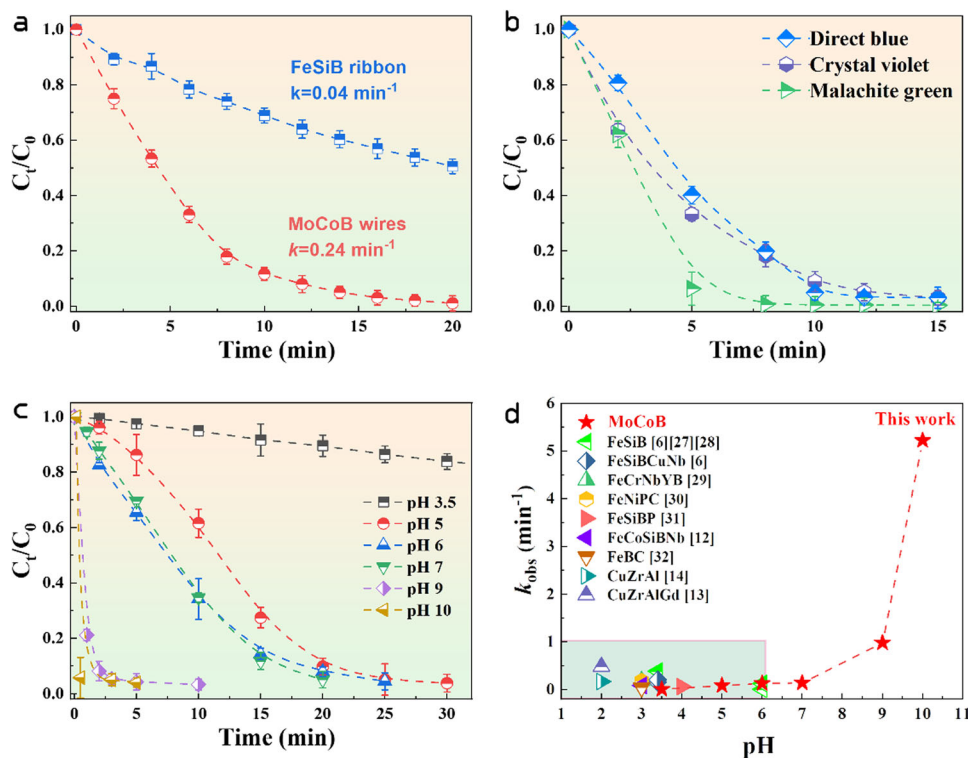
Fig. 2 Catalytic performance. a Comparison of degradation efficiency of the current MoCoB MG microwires with Fe78Si9B13 MG ribbons in CV dye. **b** Removal rate of three dyes. **c** Removal rate of CV by using the MoCoB as the catalyst under different pH value. **d** Summary plots comparing with previous literature results in terms of catalytic activity and suitable pH[9,15–17,26–31].

The adaptability of the catalyst under different conditions is of great importance. To scientifically and comprehensively evaluate the effects of temperature, pH, H_2O_2 dosage and original concentration of the solution, an orthogonal matrix L16 (4^4) was designed to cover the possible degradation effects obtained under all combinations of factors, with k_{obs} as the final indicator. It is clearly found that k_{obs} with the maximum value is shown in number 13 (Supplementary Table 2), which is the best condition for MG catalysis (i.e., the best value for multi-factor variation), and a series of subsequent degradation experimental parameters are used as a reference. Notably, we also found that pH was the main factor affecting the degradation efficiency (Supplementary Table 3). Catalytic performance for other individual environmental factors also can be seen in Supplementary Fig. 1a–d. The results show that the degradation rate accelerates continuously as the temperature increases from 293 to 333 K. Moreover, the activation energy (ΔE) can be evaluated by the Arrhenius-type Eq. (2):

$$\ln k_{obs} = -\Delta E/RT + \ln A \qquad (2)$$

where R is the gas constant, T is the temperature, and ln$A$ is the proportionality constant. The ΔE of present microwire catalysts of 44.6 KJ/mol is much lower than that of the crystalline catalysts (60–250 KJ/mol), indicating the metallic glasses are more likely to cross the reaction energy barrier for catalytic degradation reactions[25,32]. It is noticed that the degradation rate increases with increasing H_2O_2 dosage (Supplementary Fig. 1d). Unlike the conventional Fenton-like system, the current MoCoB/H_2O_2 system breaks the limitation that H_2O_2 annihilates hydroxyl radicals instead when added in excess[33–35]. As shown in Supplementary Fig. 1c, the microwire catalyst still exhibits excellent degradation ability over a wide range of concentrations. Apparently, the k_{obs} of the CV solution can be effectively improved by increasing the amount of catalyst, H_2O_2 and reaction temperature. In addition, the leached Mo/Co ion only contributed less than 10% of dye

degradation during the catalytic activity, indicating that the dye degradation was primarily derived from the contribution of the heterogeneous catalyst (Supplementary Fig. 2).

Reusability

The sustainability and stability of catalysts is one of the core issues to be considered in practical wastewater remediation. However, most of the reported metallic glasses often suffer from surface aging or product coverage during the catalytic degradation, especially after multiple cycles[9,18]. In this work, the cycling performance and long-term reactivity of the catalysts in CV solution was systematically investigated. Figure 3 shows the degradation performance of different cycles and compared with other materials, it was found that the degradation efficiency still reaches more than 80% after 46 cycles and the degradation rate always maintains at a stable level, as shown in Fig. 3a. Figure 3b summarizes the comparison graph of k_{obs} versus reusability of reported metallic glasses for wastewater remediation, with more details presented in Supplementary Table 1[9,17,28,29,31,36–39]. It can be seen that such a durable catalyst with high catalytic activity show great potential for practical wastewater treatment applications.

Reaction mechanism

The current MoCoB catalysts exhibit excellent catalytic performance in terms of catalytic activity, pH adaptation and reusability. To decode the catalytic mechanism of MoCoB MG microwires, we used different methods to analyze the degradation mechanism, Fig. 4 shows the corresponding experimental results of different methods. EPR analysis were conducted using DMPO and TEMP as the spin-trapping agents (see Fig. 4a). Surprisingly, in addition to •OH (1:2:2:1), superoxide radicals •O_2^- (1:1:1:1) was also produced during the catalytic process. It should be particularly emphasized that we also found singlet oxygen $^1O_2$ (1:1:1), which has never
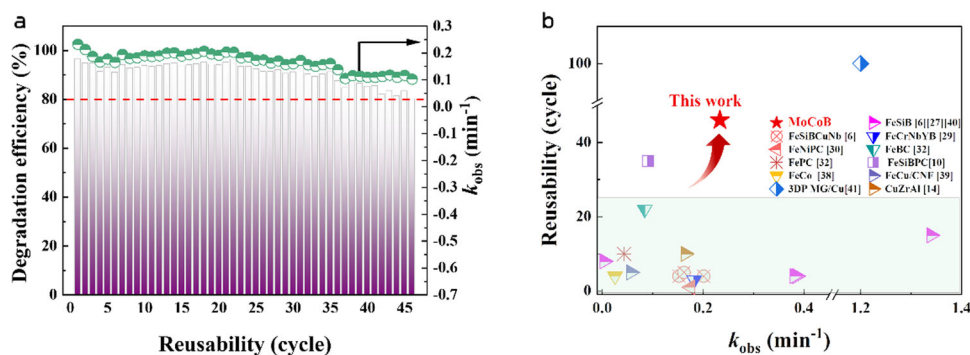
Fig. 3 The degradation performance of different cycles and compared with other materials. a Reusability of the MoCoB catalysts toward the degradation of CV and **b** comparison of the catalytic performance with previously reported catalysts in terms of kobs versus reusability.
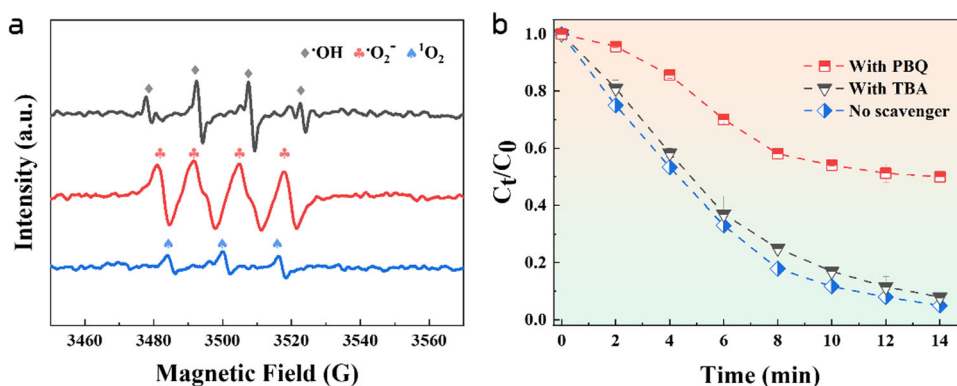

Fig. 4 The corresponding experimental results of different methods. a EPR spectra using DMPO and TEMP as trapping agents at room temperature and natural pH and **b** quenching experiments using TBA and PBQ.

been reported previously in amorphous alloy/H_2O_2 systems for wastewater treatment. To further clarify the role of each reactive intermediate in the degradation process, quenching experiments were performed with tertbutanol (TBA) and p-benzoquinone (pBQ). Strikingly, $\cdot OH$ only assumed a weak effect, while a small amount of pBQ was able to terminate more than 50% of the degradation reaction (see Fig. 4b). In other words, $\cdot O_2^-$ plays a dominant role in the whole catalytic degradation, and the advanced oxidation mechanism based on the combined action of $\cdot O_2^-$ and $^1O_2$ enables the rapid degradation of dyes. According to the Haber–Weiss cycle, $^1O_2$ is generated by the further oxidation of the reactive species $\cdot O_2^-$[40]. Moreover, with the increasing of solution pH (from 3.5–10), the content of $\cdot O_2^-$ and the rate of their deprotonation to produce $^1O_2$ are also increasing. This fully confirms the nature of the current system that degrades at a faster rate under alkaline conditions than acidic conditions, a similar phenomenon was observed in Fe_2O_3@FCNT[41]. This confirms why the current MG catalyst can function in acidic media as well as achieve rapid degradation in most alkaline conditions.

In order to gain insight into the catalytic mechanism of the MG in the degradation process, density functional theory (DFT) was applied in simulations, Fig. 5 shows the decomposition process of H_2O_2 at different sites on the amorphous surface calculated by first principles. The Mo site and Co site were chosen respectively (Fig. 5a, b). It can be concluded that once H_2O_2 is adsorbed by the catalyst, the O-O bond is rapidly elongated to form two hydroxyl radical. Under the strong oxidation of the amorphous matrix, the two $\cdot OH$ quickly turn into H_2O, which is in excellent agreement with the EPR and quenching results obtained in Fig. 4. To better understand the effect of the atoms on the catalytic process, the

absorption energy of H_2O_2 is calculated with E_{ads} (Mo) $= -0.53$ eV and E_{ads} (Co) $= -0.50$ eV, which indicates a stronger adsorption capacity of Mo atom. It can be seen from Fig. 5c that the energy is progressively lower during this process, indicating that the transition is completely spontaneous in the presence of the metallic glass catalyst. With respect to the Mo site (Fig. 5d), it was found that significant charge transfer occurs at the catalysis and O-O, respectively. The corresponding electron transfers are 0.4e and 0.6e. These findings indicate that MG catalysts provide a large electronic basis for the catalytic process. Moreover, we also found that the most stable state of O-O is in the triangular structure of Mo/Co atoms, which is once again emphasized the synergistic effect of bimetals.

To fundamentally analyze the role of Mo/Co bimetals in the excellent stability, XPS analysis of the samples were performed at different cycles, and all the results were corrected with the C peak (284.8 eV). Figure 6a shows the Mo3d pattern, wherein the Mo^0 are transformed into Mo^{4+} and Mo^{6+} in the recycling microwires. Similarly, Co^0 in the original catalysts gradually evolves to Co^{2+} and Co^{3+} as the reused (Fig. 6b). The transformation of two metallic elements indicating that the Mo^0/Co^0 is the electron supplier during the catalytic performance. Additionally, the oxidation process from Mo^{4+} to Mo^{6+} and Co^{2+} to Co^{3+} is the important process for the generation of reactive species. It is well known that from thermodynamics aspect, the higher valence is very difficult to return to the lower valence state again, which greatly limits the production of reactive species. However, in this work, a Co^{2+}-rich surface was found to be stable on the cycling catalyst because of the reductive Mo^{6+}. To confirm this issue, the ratios of two elements are purposefully summarized in Fig. 6c. As can be seen, the ratio of Mo^{4+}/Mo^{6+} and Co^{3+}/Co^{2+} gradually
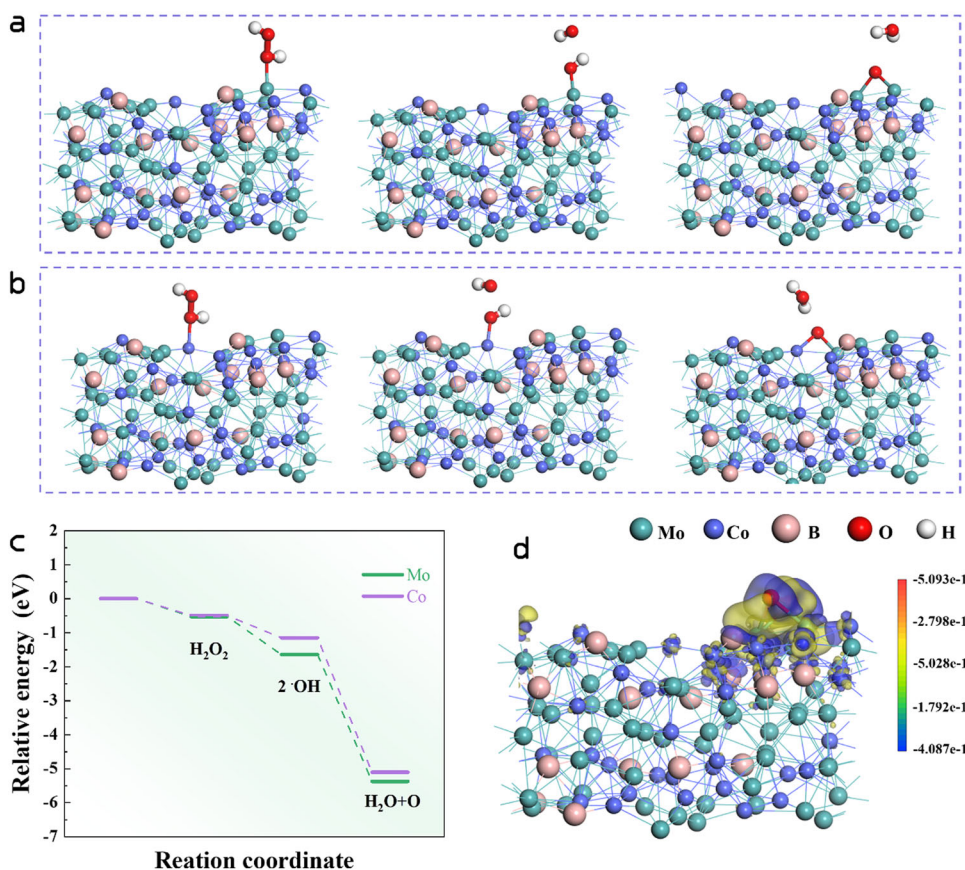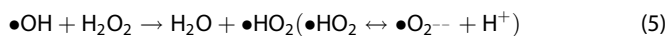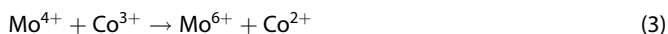
Fig. 5   The DFT calculations of the decomposition process of H₂O₂ at different sites on the catalysts surface. a Mo site, **b** Co site, **c** reaction coordinates of Mo and Co site and **d** surface structure with electron density difference plots of Mo-doped H₂O₂.

decreases with the cycles. It is worth noting that the trends in the ratios of the two metal elements are completely opposite. This implies that the stable presence of a Co^{2+}-rich surface is necessarily linked to Mo^{4+}. In other words, Mo^{4+} acts as a reducing agent and electron transfer medium to accelerate the redox cycle from Co^{3+} to Co^{2+}, as in Eq. 3. Figure 6d also shows the schematic diagram of electron transfer in the catalytic process. The bimetal forms a closed internal cycling system, which becomes the key reason for the current MoCoB MG microwire with 46 cycles. More importantly, the electron enriched MoCoB catalyst allows •OH to further react with H_2O_2 to produce $•O_2^-$ and $^1O_2$ (Eqs. 4 and 5)[42]. That is also the reason why •OH can be detected in the EPR (Fig. 4a), but does not directly degrade the wastewater.

$$Mo^{4+} + Co^{3+} \rightarrow Mo^{6+} + Co^{2+} \qquad (3)$$

$$•OH + •OH \rightarrow H_2O_2 \qquad (4)$$

$$•OH + H_2O_2 \rightarrow H_2O + •HO_2(•HO_2 \leftrightarrow •O_2^{--} + H^+) \qquad (5)$$

The long-term reactivity of the catalyst is mainly related to the chemical reaction and stability of the alloy surface. As can be seen in Fig. 7a, the MoCoB shows a stable charge-transfer resistance ($R_{ct} = 860–881 \, \Omega.cm^2$) after reused compared to the origin catalysts ($R_{ct} = 1732 \, \Omega.cm^2$). Moreover, the catalysts activated by H_2O_2 have significantly lower R_{ct}, indicating the important role of activators in stimulating catalytic activity. The double-layer capacitance (Cdl) results and electrochemical surface area (ECSA) values are shown in Fig. 7b and Supplementary Fig. 3. The ECSA result for the original catalyst was $13.8 \, \mu F/cm^2$. After 5 to 46 cycles,

the ECSA was maintained at $14.5–20.2 \, \mu F/cm^2$. Figure 7c analyzes the variation of R_{ct} and ECSA with the number of cycles. Such results reveal from an electrochemical point of view why the current MG has high reusability. Figure 7d indicates the evolution of the surface morphologies of the catalysts at different cycles, showing some rounded precipitates and nanoparticles after 5 and 10 cycles. In particular, the catalysts display a self-reconfiguration ability to its original smooth state after 46 cycles, which is mainly related to the special structure of the metallic glasses[39]. The EDS results after different cycles show a uniform distribution, except for a very small amount of Mo deprivation after 5 cycles. In particular, it should be noted that O elements did not significantly aggregate after multiple cycles, implying that the reactivity of the catalyst is not limited by the dense oxide layer.

Conclusion

In summary, the ternary MoCoB MG microwire with high specific surface area were prepared by melt spinning techniques, which showed ultra-high catalytic performance and reusability in wastewater degradation. The results show that the electron enriched Mo-based catalysts also exhibit surprisingly high stability over a wide pH range (5–10), overcoming the limitation in alkaline conditions. Due to the special amorphous structure and alloy system, Mo can accelerate the reduction process of Co^{3+} to Co^{2+} on the surface forming a bimetallic internal circulation mechanism. The catalytic mechanism and reactive species are discussed in detail both from experiments and DFT calculations, and the dominant role of $•O_2^-$ provide a perspective for the subsequent research of the metallic glasses/H_2O_2 system in wastewater treatment. It also provides insights into practical applications of
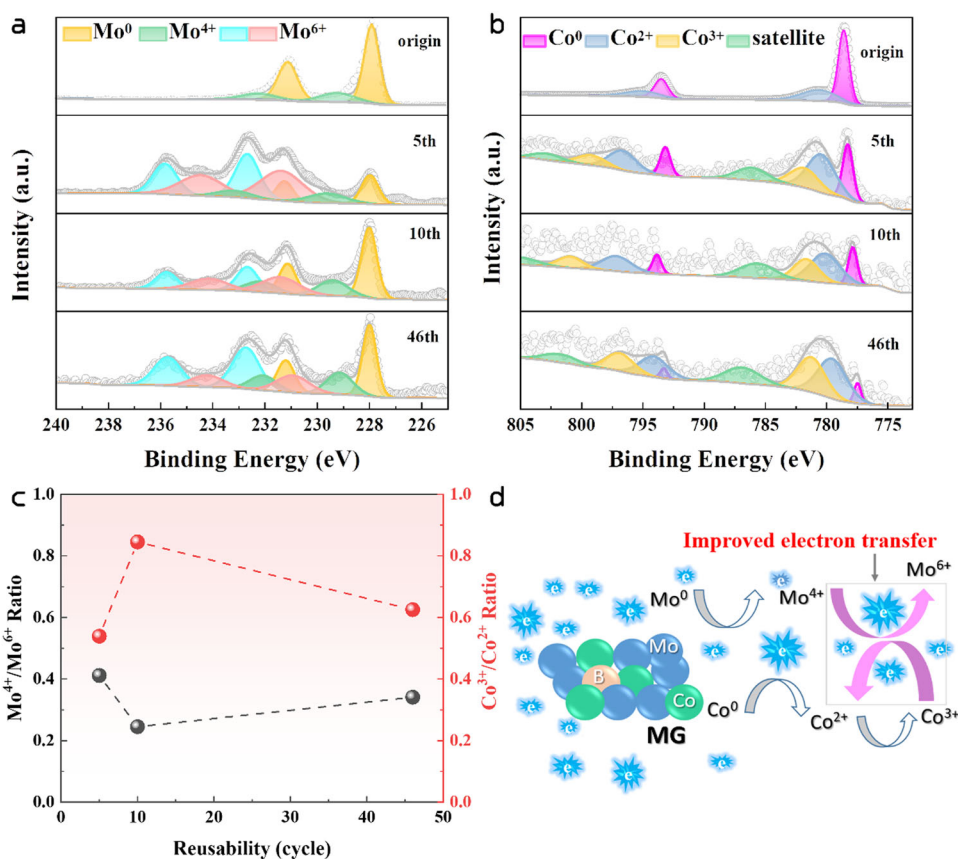
Fig. 6 XPS results of MoCoB MG microwire in different states. a Mo 3d. **b** Co 2p. **c** The ratio of different elements on the catalysts surface. **d** Schematic illustration of the electronic transfer.

MG catalysts, making Mo-based MG microwires potential candidate for environmental treatment.

METHODS

Material and fabrication process

The $Mo_{51}Co_{34}B_{15}$ (at. %) MG microwires were manufactured by melt-spinning techniques with a wire speed of ~40 m/s for copper wheels. Before that, high-purity molybdenum (99.9 wt. %), cobalt (99.9 wt. %), and boron (99.5 wt. %) were made into a master alloy ingot by arc melting, which was melted at least 5 times to ensure chemical homogeneity.

Crystal Violet ($C_{25}H_{30}ClN_3$), Malachite Green ($C_{23}H_{25}ClN_2$) and Direct Blue 6 ($C_{32}H_{20}N_6Na_4O_{14}S_4$) dyes were purchased from Chongqing Titanium New Chemical Co. The pH values of the organic solutions were adjusted with 1 M HCl and 1 M NaOH. All the reagents were analytically pure except 30% H_2O_2 without further purified.

Structure characterization method

The structure of the amorphous catalysts was characterized by X-ray diffraction (XRD, SHIMADZU XRD-6100) using Cu-Kα radiation. The thermal stability was studied by differential thermal analysis (DTA, STA409PC) under Ar_2 atmosphere at a heating rate of 20 K/min. The specific surface area of the prepared catalysts was tested by BET (JW-BK400) under N_2 atmosphere.

Catalytic experiment method

During the catalytic experiments, the temperature of the solution was controlled with a water bath and magnetic stirring was maintained. During the reaction, 3 mL of the solution was drawn with a syringe at predetermined time intervals (e.g., 2, 5, 10, 12, 15 min, etc.) and the absorbance of the corresponding solution was measured with a UV-visible photometer (Spectrophotometer U-3310). The reusability of the samples was assessed by cycling experiments, which was performed in 20 ppm of CV solution. After one cycle, the catalysts were removed and washed three times with deionized water, then blown dry and continued in a fresh CV solution to start the next cycle, repeating this process until a significant change in catalytic efficiency was observed. Molybdenum chloride ($MoCl_5$) and cobalt chloride hexahydrate ($CoCl_2.6H_2O$) were employed as homogeneous catalysts to assess the effect of leached metal ions on the degradation of the dye during the catalytic process. The concentration of metal ions was measured by inductively coupled plasma atomic emission spectrometry (ICP- OES, OPTIMA 8000DV).

The effect of external factors including temperature, pH value, H_2O_2 dosage and concentration of the solution on the catalytic performance was evaluated using an orthogonal experimental system. If not specifically mentioned, the following conditions were chosen: dye concentration of 20 ppm, catalyst dosage of 2 g/L, H_2O_2 addition of 0.1 M, and temperature of 323 K. The electrochemical impedance and cyclic voltammetry curve of the samples were tested in CV solution using a standard three-electrode system consisting of a Pt electrode, a saturated calomel electrode, and the catalysts. The surface morphologies and elemental distribution of the catalysts before and after the reaction were observed by scanning electron microscopy (SEM, JSM-6610) with energy spectrum analysis (EDS). Then, the reaction mechanism was comprehensively and deeply analyzed by X-ray photoelectron spectroscopy (XPS, AXIS SUPRA+) and electron paramagnetic resonance (EPR, EMXplus-9.5/12).
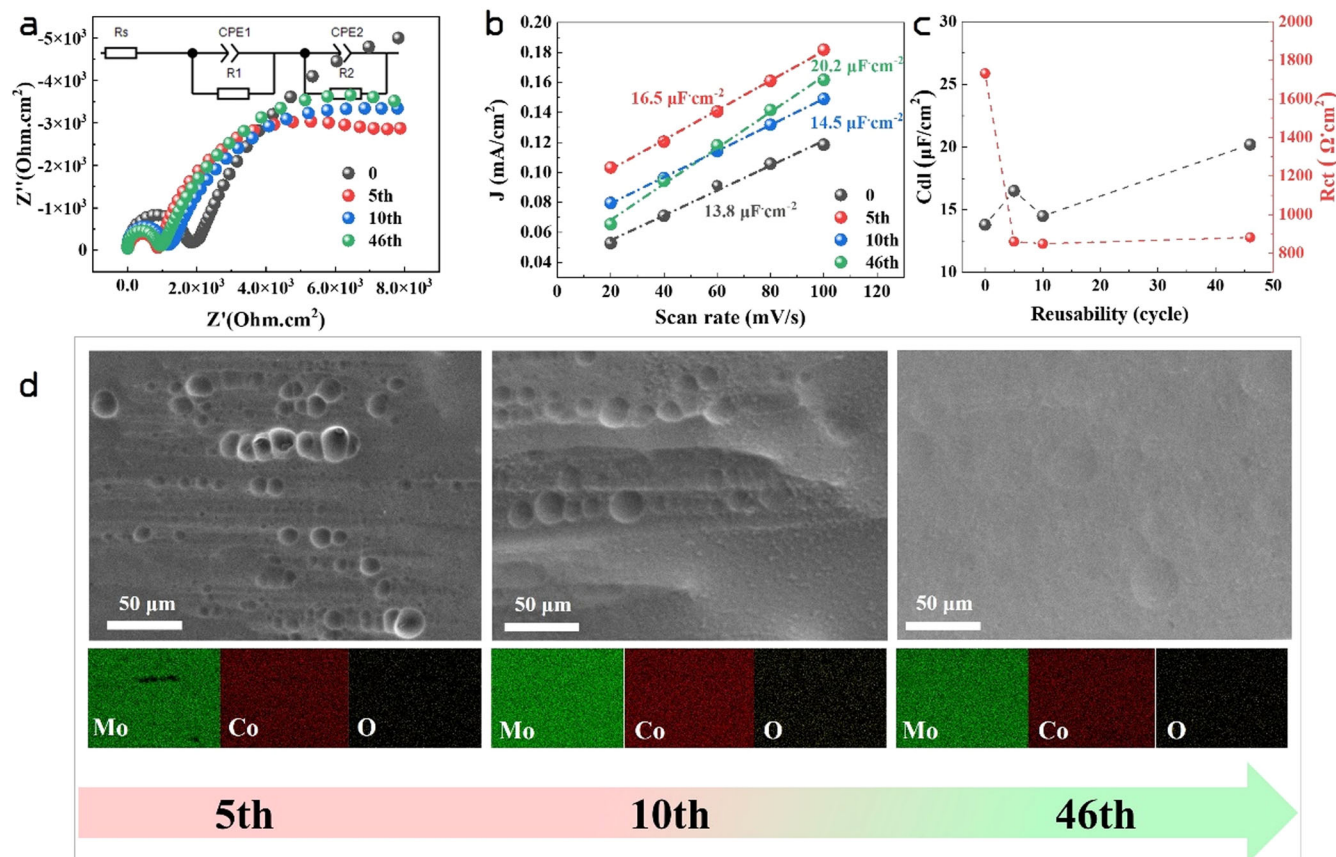
Fig. 7 Electrochemical curves of the original sample and the sample after degradation with different number of cycles. a EIS curve. **b** Cdl calculated from cyclic voltammetric curves. All electrochemical tests were performed in 20 ppm CV solution. **c** Variation of Rct and Cdl under different cycles. **d** Surface morphologies and elemental mapping results of MG microwire after different cycles.

First-principles calculation process

The First-Principles Calculations were performed by the CASTEP module. The projector augmented wave (PAW) pseudopotential was adopted for the comprehensive density functional theory (DFT) calculations, and the generalized gradient approximation (GGA) using Perdew–Burke–Ernzerhof (PBE) was applied for the description of the electron exchange correlation[43,44]. The structure of MoCoB MG was built by Ab initio molecular dynamics (AIMD) simulations via a traditional melted and quenched process. The k points of Monkhorst–Pack was set to be $2 \times 3 \times 1$ and the energy cutoff was set to be 300 eV, and a DFT-D approach with the Ortmann–Bechstedt–Schmidt (OBS) vdW correction was selected to take into account vdW interactions[45,46]. The energy and maximum force convergence criteria during geometry optimizations were set at 10^{-5} eV /atom and 0.03 eV/Å, respectively, and a vacuum zone measuring 25 Å was applied to prevent the interaction between periodical layers.

DATA AVAILABILITY
The authors declare that the data supporting the findings of this study are included within the paper and available from the corresponding author on reasonable request.

REFERENCES
1. Wang, W. H. Bulk metallic glasses with functional physical properties. *Adv. Mater.* **21**, 4524–4544 (2009).
2. Hu, Y. C. et al. A highly efficient and self-stabilizing metallic-glass catalyst for electrochemical hydrogen generation. *Adv. Mater.* **28**, 10293–10297 (2016).
3. Wang, Z. J. et al. Low-iridium-content IrNiTa metallic glass films as intrinsically active catalysts for hydrogen evolution reaction. *Adv. Mater.* **32**, e1906384 (2020).
4. Hu, F. et al. Amorphous metallic NiFeP: a conductive bulk material achieving high activity for oxygen evolution reaction in both alkaline and acidic media. *Adv. Mater.* **29**, 1606570 (2017).
5. Liang, S. X. et al. Selective laser melting manufactured porous Fe -based metallic glass matrix composite with remarkable catalytic activity and reusability. *Appl. Mater. Today* **19**, 100543 (2020).
6. Liang, S. X. et al. Compelling rejuvenated catalytic performance in metallic glasses. *Adv. Mater.* **30**, 1802764 (2018).
7. Liang, S. X. et al. A laser-based synthesis route for magnetic metallic glass nanoparticles. *Scr. Mater.* **203**, 114094 (2021).
8. Wang, J. Q. et al. Rapid degradation of azo dye by fe-based metallic glass powder. *Adv. Funct. Mater.* **22**, 2567–2570 (2012).
9. Jia, Z. et al. Surface aging behaviour of Fe-based amorphous alloys as catalysts during heterogeneous photo Fenton-like process for water treatment. *Appl. Catal. B Environ.* **204**, 537–547 (2017).
10. Jia, Z. et al. Disordered atomic packing structure of metallic glass: toward ultrafast hydroxyl radicals production rate and strong electron transfer ability in catalytic performance. *Adv. Funct. Mater.* **27**, 1702258 (2017).
11. Tang, Y. et al. Insight into the high reactivity of commercial Fe-Si-B amorphous zero-valent iron in degrading azo dye solutions. *RSC Adv.* **5**, 34032–34039 (2015).
12. Chen, S. Q. et al. Excellent long-term reactivity of inhomogeneous nanoscale Fe-based metallic glass in wastewater purification. *Sci. China Mater.* **63**, 453–466 (2020).
13. Jia, Z. et al. Attractive in situ self-reconstructed hierarchical gradient structure of metallic glass for high efficiency and remarkable stability in catalytic performance. *Adv. Funct. Mater.* **29**, 1807857 (2019).
14. Jia, Z. et al. Amorphous Fe78Si9B13 alloy: an efficient and reusable photo-enhanced Fenton-like catalyst in degradation of cibacron brilliant red 3B-A dye under UV–vis light. *Appl. Catal. B Environ.* **192**, 46–56 (2016).

15. Jiang, J. L. et al. Synergistic function of iron and cobalt in metallic glasses for highly improving persulfate activation in water treatment. *J. Alloy. Compd.* **822**, 153574 (2020).

16. Li, Z. et al. Cu-based metallic glass with robust activity and sustainability for wastewater treatment. *J. Mater. Chem. A* **8**, 10855–10864 (2020).

17. Zhao, B. et al. Highly efficient and stable CuZr-based metallic glassy catalysts for azo dye degradation. *J. Mater. Sci. Technol.* **46**, 88–97 (2020).

18. Wang, Q. et al. Investigation of FePC amorphous alloys with self-renewing behaviour for highly efficient decolorization of methylene blue. *J. Mater. Chem. A* **6**, 10686–10699 (2018).

19. Wang, P. et al. Fast decolorization of azo dyes in both alkaline and acidic solutions by Al-based metallic glasses. *J. Alloy. Compd.* **701**, 759–767 (2017).

20. Lai, L. et al. High-temperature Mo-based bulk metallic glasses. *Scr. Mater.* **203**, 114095 (2021).

21. Lai, L. M. et al. Ternary Co-Mo-B bulk metallic glasses with ultrahigh strength and good ductility. *J. Non-Cryst. Solids* **524**, 119657 (2019).

22. Song, X. C. et al. Ultrasonic welding of Fe78Si9B13 metallic glass. *Mater. Sci. Forum* **809**–**810**, 348–353 (2015).

23. Li, R. et al. Flexible glassy grid structure for rapid degradation of azo dye. *Mater. Des.* **155**, 346–351 (2018).

24. Zhao, B. et al. Performance enhancement and catalytic mechanism identification of Cu-based composite for degradation of organic contaminants. *Powder Technol.* **389**, 11–20 (2021).

25. Zhang, L. C. et al. A review of catalytic performance of metallic glasses in wastewater treatment: recent progress and prospects. *Prog. Mater. Sci.* **105**, 100576 (2019).

26. Liu, P. et al. Synthesis of an Fe rich amorphous structure with a catalytic effect to rapidly decolorize Azo dye at room temperature. *ACS Appl Mater. Interfaces* **6**, 5500–5505 (2014).

27. Zhang, C. et al. Rapid reductive degradation of azo dyes by a unique structure of amorphous alloys. *Chin. Sci. Bull.* **56**, 3988–3992 (2011).

28. Yang, W. et al. A novel thermal-tuning Fe-based amorphous alloy for automatically recycled methylene blue degradation. *Mater. Des.* **161**, 136–146 (2019).

29. Liang, S. X. et al. Surface reactivation of FeNiPC metallic glass: a strategy for highly enhanced catalytic behavior. *J. Phys. Chem. Solids* **132**, 89–98 (2019).

30. Deng, Z. et al. Fe-based metallic glass catalyst with nanoporous surface for azo dye degradation. *Chemosphere* **174**, 76–81 (2017).

31. Miao, F. et al. Excellent reusability of FeBC amorphous ribbons induced by progressive formation of through-pore structure during acid orange 7 C degradation. *J. Mater. Sci. Technol.* **38**, 107–118 (2020).

32. Yang, Y. et al. The preparation of Fe_2O_3-ZSM-5 catalysts by metal-organic chemical vapour deposition method for catalytic wet peroxide oxidation of m-cresol. *R. Soc. Open Sci.* **5**, 171731 (2018).

33. Jia, Z. et al. Heterogeneous photo Fenton-like degradation of cibacron brilliant red 3B-A dye using amorphous $Fe_{78}Si_9B_{13}$ and $Fe_{73.5}Si_{13.5}B_9Cu_1Nb_3$ alloys: the influence of adsorption. *J. Taiwan Inst. Chem. Eng.* **71**, 128–136 (2017).

34. Yin, Y. et al. Ultrafine copper nanoclusters and single sites for Fenton-like reactions with high atom utilities. *Environ. Sci. Nano* **7**, 2595–2606 (2020).

35. Liang, S. X. et al. Tailoring surface morphology of heterostructured iron-based Fenton catalyst for highly improved catalytic activity. *J. Colloid Interface Sci.* **581**, 860–873 (2021).

36. Ganiyu, S. O. et al. A hierarchical CoFe-layered double hydroxide modified carbon-felt cathode for heterogeneous electro-Fenton process. *J. Mater. Chem. A* **5**, 3655–3666 (2017).

37. Wang, J. et al. In-situ incorporation of iron-copper bimetallic particles in electrospun carbon nanofibers as an efficient Fenton catalyst. *Appl. Catal. B Environ.* **207**, 316–325 (2017).

38. Ge, Y. X. et al. Remarkably enhanced Fenton-like catalytic activity and recyclability of Fe-based metallic glass by alternating magnetic field: mechanisms and industrial applications. *J. Mater. Chem. A* **10**, 23314–23322 (2022).

39. Yang, C. et al. Three-dimensional hierarchical porous structures of metallic glass/copper composite catalysts by 3D printing for efficient wastewater treatments. *ACS Appl. Mater. Interfaces* **13**, 7227–7237 (2021).

40. Khan, A. U. et al. Singlet molecular oxygen in the Haber-Weiss reaction. *Proc. Natl Acad. Sci. USA* **91**, 12365–12367 (1994).

41. Yang, Z. et al. Singlet oxygen mediated iron-based Fenton-like catalysis under nanoconfinement. *Proc. Natl Acad. Sci. USA* **116**, 6659–6664 (2019).

42. Zhao, M. et al. MoS2 co-catalysis promoted CaO_2 Fenton-like process: performance and mechanism. *Sep. Purif. Technol.* **276**, 119289 (2021).

43. Perdew, J. P. et al. Generalized gradient approximation made simple. *Phys. Rev. Lett.* **77**, 3865 (1996).

44. Perdew, J. P. et al. Atoms, molecules, solids, and surfaces: applications of the generalized gradient approximation for exchange and correlation. *Phys. Rev. B* **46**, 6671 (1992).

45. Ortmann, F. et al. Semiempirical van der Waals correction to the density functional description of solids and molecular structures. *Phys. Rev. B* **73**, 205101 (2006).

46. Li, C. et al. Theoretical anchoring effect of new phosphorus allotropes for lithium–sulfur batteries. *Nanoscale* **12**, 11095–11111 (2020).

ACKNOWLEDGEMENTS

AUTHOR CONTRIBUTIONS

M.T.: validation, investigation, data curation, methodology, formal analysis, writing—original draft preparation, visualization. L.L.: methodology, data curation, visualization, investigation. C.S.: validation, investigation. C.L.: software. C.Z.: investigation, writing—reviewing and editing. S.G.: supervision, conceptualization, methodology, writing—reviewing and editing, funding acquisition.

COMPETING INTERESTS

The authors declare no competing interests.

ADDITIONAL INFORMATION

Supplementary information The online version contains supplementary material available at https://doi.org/10.1038/s41529-023-00390-1.

Correspondence and requests for materials should be addressed to Cheng Zhang or Shengfeng Guo.

Reprints and permission information is available at http://www.nature.com/reprints

Publisher's note Springer Nature remains neutral with regard to jurisdictional claims in published maps and institutional affiliations.